Journal of Hazardous Materials 385 (2020) 121520

Contents lists available at ScienceDirect

Journal of Hazardous Materials

journal homepage: www.elsevier.com/locate/jhazmat

Variable surface charge of humic acid-ferrihydrite composite: Influence of electrolytes on ciprofloxacin adsorption

Cristian Urdiales[a], Manuel Gacitua[b], Loreto Villacura[c], Carmen Pizarro[b,d,**], Mauricio Escudey[b,d], Camila Canales[e], Mónica Antilén[a,d,*]

[a] Pontificia Universidad Católica de Chile, Facultad de Química y de Farmacia, Vicuña Mackenna 4860, Santiago, 7820436, Chile
[b] Universidad de Santiago de Chile, Facultad de Química y Biología, USaCh, Av. L.B. O'Higgins 3363, Santiago, 7254758, Chile
[c] Universidad de Chile, Facultad de Ciencias, Las Palmeras 3425, Santiago, 7800024, Chile
[d] Centro para el Desarrollo de la Nanociencia y Nanotecnologia (CEDENNA), Av. L.B. O'Higgins 3363, Santiago, 7254758, Chile
[e] Pontificia Universidad Católica de Chile, Escuela de Ingeniería, Departamento de Ingeniería Hidraúlica y Ambiental, Vicuña Mackenna 4860, Santiago, 7820436, Chile

GRAPHICAL ABSTRACT

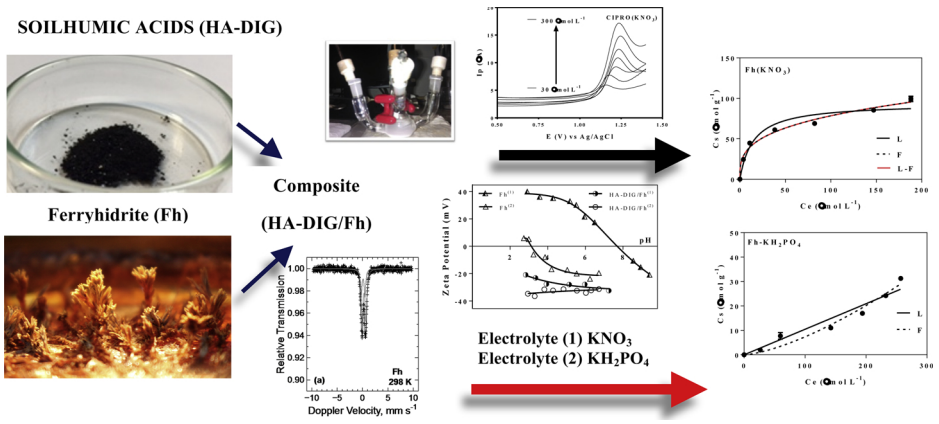

ARTICLE INFO

Editor: Deyi Hou

Keywords:
Antibiotics
Natural organic matter
Iron oxides
Mössbauer spectroscopy
Sorption models

ABSTRACT

Antimicrobial compounds are found in a range of environments as pollutants. Here, we evaluated the influence of two common anions, NO_3^- and PO_4^{3-}, on ciprofloxacin adsorption on humic acid/ferrihydrite composite (HA-DIG/Fh), synthetic ferrihydrite (Fh), and humic acid (HA-DIG) under controlled pH (7.0), ionic strength (0.1 M) and temperature (25 °C). All materials were characterized by isoelectric point (IEP), while the composite and the iron oxide were characterized by Mössbauer spectroscopy. Kinetic and isotherm adsorption studies were carried out using cyclic voltammetry (in KH_2PO_4) and square wave voltammetry (in KNO_3). The application of kinetic models for both anions revealed Fh to fit to a pseudo second order model ($R^2 = 0.941$); while HA-DIG ($R^2 = 0.950$) and HA-DIG/Fh ($R^2 = 0.993$) were fitted to pseudo first order models. The adsorption results showed a high dependency electrolyte, especially in Fh, where different shape curves (H-type in KNO_3 and C-type in KH_2PO_4) and maximum experimental adsorbed amount C_m were observed. This finding is supported by the distinct IEP values and change in sign of surface charge between the two ions. Finally, results suggest that

* Corresponding author at: Facultad de Química y de Farmacia, Pontificia Universidad Católica de Chile, Vicuña Mackenna 4860, 7820436, Santiago, Chile.
** Corresponding author at: Facultad de Química y Biología, Universidad de Santiago de Chile, Av. L.B. O'Higgins 3363, Santiago, 7254758, Chile.
E-mail addresses: cgurdiales@uc.cl (C. Urdiales), manuel.gacitua@usach.cl (M. Gacitua), loretovillacura@gmail.com (L. Villacura), carmen.pizarro@usach.cl (C. Pizarro), mauricio.escudey@usach.cl (M. Escudey), cicanale@uc.cl (C. Canales), mantilen@uc.cl (M. Antilén).

https://doi.org/10.1016/j.jhazmat.2019.121520
Received 30 July 2019; Received in revised form 16 October 2019; Accepted 21 October 2019
Available online 17 November 2019

HA-DIG could be potentially used in environmental remediation to remove antibiotics from natural matrices, though the risk of antibiotic transportation increased with depth in the soil profile.

1. Introduction

The impacts of antimicrobial compounds in environmental matrices such as soil and water have become a global concern. International entities such as the World Health Organization (WHO) and Food and Agriculture Organization (FAO) have expressed their concerns regarding the eventual risks from extensive use of antibiotics in animal agriculture for both therapeutic purposes and growth promotion (Fao et al., 2013). Use of antimicrobial compounds introduces a selection pressure for resistant microorganisms, among which human and animal pathogens are of primary concern (Charuaud et al., 2019). The consequences of excessive antimicrobial use are not contained to animal hosts, but rather extend to the environment. Globally, manure application is a common agricultural practice that serves to recycle key nutrients (Albero et al., 2018), but application of antibiotic-polluted manure represents a pathway for these compounds to enter environmental matrices. Upon incorporation on the superficial horizons of soils, antimicrobials may be adsorbed, accumulated (Jacobsen et al., 2004), and leached through an array of transport mechanisms (Lindsey et al., 2001; Kolpin et al., 2002), where their fate may pose consequences to human and environmental health (Boxall et al., 2003).

Questions regarding the fate and transport of antimicrobial compounds in the environment have stimulated considerable original research over the last two decades. It is well-established that adsorption processes significantly influence the transport, fate and bioavailability of most organic pollutant in soils. There are numerous reports regarding immobilization of antibiotics using different adsorbents like activated carbon (Ahmed, 2017; Fu et al., 2017), magnetite/carbon composites (Jiang et al., 2016), mesoporous silica (Liang et al., 2016), poultry litter (Liu et al., 2013), and natural aluminosilicate minerals (Wu et al., 2013), among other surfaces. Studies have revealed that antibiotics like tetracycline strongly interact with clay minerals and hydrated oxides from soils, promoting accumulation (Figueroa et al., 2004; Gu and Karthikeyan, 2005a). On the other hand, soil organic matter (SOM), especially in high concentrations, may facilitate organic pollutant transport through soils and water bodies (John et al., 1989). Therefore, SOM content may not only promote the transport of organic compounds such as tetracycline, sulphonamide, and quinolones (Thiele-Bruhn and Beck, 2005), but also serve as an important adsorbent phase for organic pollutants (Essington, 2004). Among SOM constituents, humic acids (HA) are notable for their surfactant properties and multi-functionality (Wershaw et al., 1977). These properties of HA are thought to influence antibiotic–OM interactions, as they may interact with both non-polar and polar functional groups of antibiotics, yielding micelle-like aggregates. For example, HA extracted from Chilean volcanic soils has demonstrated significant ciprofloxacin adsorption capacity (Antilen et al., 2016). In addition to SOM constituents, iron oxides represent another soil component that may affect the fate of organic compounds such as antibiotics. Compounds such as oxytetracycline have been shown to act as ligands in the formation of surface complexes with some iron oxide minerals like goethite and hematite (Figueroa et al., 2004). Previous work indicates that at a pH where the ciprofloxacin (CIPRO) zwitterion form predominates, iron oxides may strongly interact with moieties present in hydrated oxides of Fe and Al surfaces through the formation of surface complexes (Gu and Karthikeyan, 2005b). In line with this observation, the widely used aquaculture antibiotic oxolinic acid has demonstrated good retention over synthetic goethite (α-FeOOH) and akaganeíte (β-FeOOH) minerals at pH 9.6 (Marsac et al., 2016). Moreover, studies carried out on magnetite nanoparticles coated with HA have shown enhanced protein adsorption-capacities compared to bare magnetite nanoparticles (Bayrakci et al., 2014)

Taken together, these reports indicate that humic acid/iron oxide composites offer to combine the multifunctionality of HA with the antibiotic adsorption capacity of iron oxides, enhancing overall adsorption. Understanding the antibiotic adsorption process to maximize adsorption efficiency requires consideration of the soil solution as a whole, including electrolytes. Nitrate anions are present in the extracts of fertile soils with low humidity, simulating minimum conditions (*wilting percentage*) for plant growth, as reported by Magistad and Reitemeier (1943). Phosphates (PO_4^{3-}) are present due to intensive use of soil P fertilization, but in comparatively lower concentrations considering the crop P requirements (Anderson et al., 1974). In volcanic ash derived soils in particular, PO_4^{3-} strongly compete with other species for adsorption sites, changing the chemical-physical properties of soils.

In this work, we measured the ciprofloxacin adsorption efficiency of three materials: humic acid/ferrihydrite composite (HA-DIG/Fh), synthetic ferrihydrite (Fh), and humic acid (HA-DIG) using adsorption kinetics and adsorption isotherms assays. In an effort to stimulate realistic environmental conditions, we also considered the influence of phosphate and nitrate anions present in the soil solution, specifically in relation to generation of variable surface charge. This work presents a one-to-one evaluation of the effect of singular physicochemical surface properties on ciprofloxacin adsorption under different soil-solution conditions. Results from this work can be used to inform material selection for removal of antimicrobials from environmental matrices.

2. Materials and methods

2.1. Samples

2.1.1. Soil

The soil sample was collected at a 0 to 0.20 m depth of uncultivated areas of Diguillin (Andisol) in southern Chile (36°53' S 72°10' W). The sample was air dried and sieved through a 2.0 mm mesh sieve.

2.1.2. Humic acid extraction

Humic acid was extracted from Diguillin soil (HA-DIG) using IHSS recommended procedure (Watanabe and Kuwatsuka, 1991) as previously described (Urdiales et al., 2018).

2.1.3. Humic acid /ferrihydrite composite synthesis

Ferrihydrite was synthesized using the procedure proposed by Schwertmann and Cornell (2000). To synthesize the composite, 8 g of $Fe(NO_3)_3 \cdot 9H_2O$ was dissolved and diluted to 100.0 mL in a volumetric flask. This solution was mixed with 50 mL of 1.0 mol L^{-1} KOH solution under vigorous stirring and left to react for 5 min. Next, with pH control, dropwise additions of alternating 1.0 or 0.1 mol L^{-1} KOH solutions were made until the formation of a dark-red solid ferrihydrite (Fh). Upon observation of the solid, 5 g of HA-DIG was added. The resulting suspension was left to settle and excess liquid was removed. The final product was washed and excess electrolytes were eliminated with distilled water using a dialysis tube. The HA-DIG/Fh composite was then obtained with a freeze dryer (Labconco 2.5 ®).

2.2. Characterization

2.2.1. Mössbauer spectroscopy

Iron oxide structures were characterized using room temperature ^{57}Fe-Mössbauer spectroscopy measurements in constant acceleration

transmission mode, with ~30 mCi ^{57}Co/Rh. Isomeric shifts were referred to α-Fe and the experimental data were fitted using Lorentzian functions with the least squares fitting procedure based on the NORMOSTM computer program.

The ^{57}Fe Mössbauer spectroscopy detects hyperfine effects at the nuclear level associated with the environment of the Fe atom when a radioactive source of ^{57}Co is used. This technique helps to establish not only iron oxidation states but also isomorphic substitutions, magnetic properties and mineralogy of iron present in a sample.

2.2.2. Particle size distribution

To determine the particle size distribution for each adsorbent, the pipette method analysis was used (Bouyoucos, 1934).

2.2.3. Isoelectric point (IEP)

Surface charge was determined by means of electrophoretic mobility studies using a Zeta Meter equipment. A suspension of 10 mg of sample in 200 mL of distilled water and 2 mL of KNO_3 or KH_2PO_4 0.1 mol L^{-1} was used. The pH (in the range 3–7) was adjusted with HNO_3 (H_3PO_4) and KOH (10^{-2} M), and electrophoretic mobility (EM) measurements were performed in a Zetameter (ZM-77). Each electrophoretic mobility value represents the average of at least 20 measurements. The zeta potential (ZP) in mV was calculated from EM data by the Helmholtz-Smoluchowski equation. The IEP was obtained from a ZP vs. pH plot.

2.2.4. Surface specific area

Surface specific area (SSA, BET area) and pore diameter were determined from the N_2 adsorption-desorption isotherms, carried out in a Micromeritics model 3Flex-MS 2010.

2.3. Electrochemical setup

The electrochemical measurements were recorded using a CH Instruments potentiostat, model 620D and a three-compartment cell. The working electrode consisted of a glassy carbon electrode with 0.07 cm^2 of exposed surface; whereas a Ag/AgCl electrode was used in a saturated solution of potassium chloride (Ag | AgCl, KCl) as a reference electrode and a spiral platinum wire (large surface area) as an auxiliary electrode. The electrochemical studies were carried out using a 3-compartment glass cell. Solutions were purged with high purity argon gas for at least 20 min. Before each measurement, the working electrode was cleaned by polishing the exposed area on a felt pad surface with a 0.3 μm alumina suspension. The electrode was subsequently rinsed with distilled water and put into an ultrasound bath to remove the remaining alumina for 60 s. Finally, before carrying out a measurement, a potential sweep of 20 cycles was carried out between -0.7 and 0.7 V in a 0.1 M NaOH solution previously purged with argon (20 min) in order to obtain a characteristic voltammetric profile in which no faradic signals were detected, and all unknown substances were removed.

Next, cyclic voltammetry (CV) and square wave voltammetry (SWV) techniques were used and adapted for quantifying the antibiotic in KNO_3 and KH_2PO_4, respectively. Previous studies (Antilen et al., 2016) established that ciprofloxacin could be oxidized onto glassy carbon electrodes when an overpotential of 1.0 V vs Ag|AgCl electrode at pH = 7.0 is applied using CV as technique. The electrochemical quantification of ciprofloxacin was carried out by CV at pH = 7.0 using 0.1 M KH_2PO_4 (PBS) as supporting electrolyte, and by SWV at pH = 7.0 and 0.1 M KNO_3 as supporting electrolyte. Then, the CIPRO concentration was determined through a calibration curve that correlates the peak current density (obtained from the CV profiles) with the variation of the antibiotic concentration (from 30 to 300 μmol L^{-1} in PBS). A calibration curve was obtained at the same concentration range of KNO_3 by using SWV at a potential window between 0.4 and 1.4 V, with parameters of amplitude, increment and frequency of 0.025 V, 0.004 V and 10 Hz, respectively.

For determining adsorptive characteristics of materials, kinetics and adsorption isotherms were obtained using the cyclic voltammetry and square wave voltammetry for antibiotic quantification in PBS and KNO_3 solution, respectively.

2.4. Kinetic studies

Kinetic experiments demonstrated requirement of an equilibration time. Equilibration was achieved using 10 mg of solid (Fh, HA-DIG and HA-DIG/Fh) suspended in a solution containing 300 μmol L^{-1} of CIPRO in 0.1 M PBS or KNO_3 in the 10 mL electrochemical cell for measurements ranging from 0.5 up to 90 min-for Fh and HA-DIG; and 0.5 up to 180 min, only for HA-DIG/Fh (PBS) as adsorption time. The pH values were measured at the end of all experiments. Equilibrium CIPRO concentration (C_e) was determined by means of the calibration curve previously described. Then, the concentration at different times (C_t) was adjusted to the pseudo first- and pseudo-second order kinetic adsorption models.

2.5. Adsorption isotherms

The adsorption isotherms of CIPRO were performed by suspending 10 mg of adsorbent in 10 mL of CIPRO solution in 0.1 M PBS or KNO_3 into the electrochemical cell. The pH values were measured at the end of all experiments. CIPRO concentration ranged from 30 to 300 μmol L^{-1}. The suspension was equilibrated for 45, 60 or 90 min for Fh, HA-DIG and HA-DIG/Fh, respectively, flushing argon throughout the end of the experiment. CV oxidation peak potential at 1.0 V vs Ag|AgCl for PBS and SWV peak at 1.25 V for KNO_3 solution were used for quantification of CIPRO equilibrium concentration in solution (C_e). Prior to and between each experiment, the working electrode was cleaned and polished using a felt pad as described above. Experimental adsorbed CIPRO concentration (C_s) vs equilibrium concentration isotherms were fitted using the Langmuir, Freundlich, and Dubinin-Radushkevich models.

2.6. Models

2.6.1. Sorption kinetic models

Pseudo-first-order (Lagergren, 1898) and *Pseudo-second-order* (Ho and McKay, 1999) kinetic models were considered to establish the kinetic theoretical parameters, using equations and their parameter definitions previously described (Antilen et al., 2016).

2.6.2. Adsorption models

The Freundlich, Langmuir, and Dubinin-Radushkevich, models (Evangelou, 1998; Freundlich, 1906; Langmuir, 1918; Misra, 1969) were used to fit the experimental data.

3. Results and discussion

3.1. Chemical characterization of adsorbents

Humic acid was extracted from Diguillin, a volcanic ash-derived soil series (Andisol). The starting soil sample had 12.5 % of organic matter contents contributing to the typical variable surface charge characteristic for this type of soil. The clay-size soil fraction of Diguillin presents a mineralogy dominated by low crystalline degree species like allophane (Escudey et al., 2001). Approximately 8.1 % of the total organic matter content of Diguillin corresponds exclusively to humic acid (HA-DIG).

Ferrihydrite and humic acid/ferrihydrite composite (HA-DIG/Fh) were characterized by ^{57}Fe Mössbauer Spectroscopy. The spectra for synthesized ferrihydrite (Fh) and HA-DIG/Fh are presented in Fig. 1. The Mössbauer spectrum of iron oxide at room temperature (Fig. 1a) confirms the presence of ferrihydrite. The intense central doublet signal is characteristic of ferrihydrite type structure and belongs to

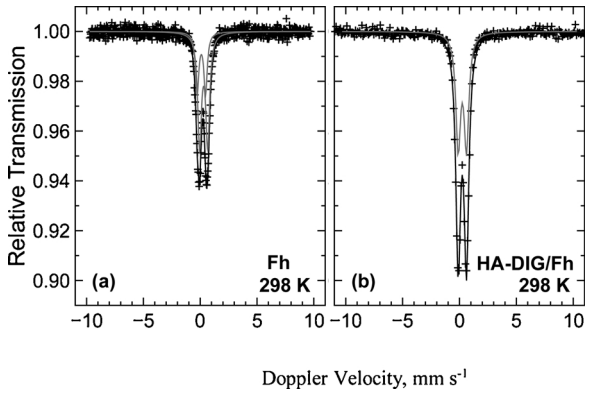

Fig. 1. ^{57}Fe Mössbauer spectra for (a) Fh, (b) HA-DIG/Fh at room temperature.

paramagnetic Fe^{+3} signal, which can be fitted employing a double-doublet model with an isomeric shift, δ, of 0.41 and 0.21 mm s^{-1} and a quadrupole splitting, ΔEQ, of 0.72 and 0.74 mm s^{-1}, respectively (Vandenberghe et al., 1990).

The Mössbauer spectrum of the composite formed between ferrihydrite and humic acid, HA-DIG/Fh, at room temperature (Fig. 1b) is similar to pure ferrihydrite, but the central doublet belonging to paramagnetic Fe^{+3} is more intense. The central doublet observed for the composite due to paramagnetic Fe^{+3} is the result of contribution of ferrihydrite and the iron compounds present in the Diguillin soil base substrate, resulting in a stronger signal than for pure ferrihydrite, which is possible to observe in the deconvolution of the Mössbauer spectrum for the HA-DG / Fh sample. In fact, the Fe:OC (organic carbon) ratio was determined (1: 2.4, respectively), while that AA (atomic absorption) measurements confirmed the presence of Fe in composite (23.7 %) and in HA (0.23 %). Model fitting in this case involved a single doublet with fitting parameters δ of 0.34 mm s^{-1} and ΔEQ of 0.72, respectively. This spectrum in which the ferrihydrite structure is maintained confirmed successful preparation of the composite.

Zeta Potential vs pH curves for Fh and HA-DIG/Fh reveal a strong dependency on the surface charge with the pH variation, as expected for a low-crystalline iron oxide (Fig. 2).

The nitrate and phosphate anions demonstrated distinct effects on the ZP vs pH curve as well as on the isoelectric point (Fig. 2). Considering that nitrate has no important interactions with Fh active surface sites, acting instead as an indifferent electrolyte, the IEP observed (7.6) can be considered as the actual IEP of ferrihydrite. Conversely, since PO_4^{3-} is known to form inner sphere complexes with active sites of ferrihydrite, the IEP of Fh in this media (3.2), is clearly affected by the adsorption of phosphate which increases the negative surface charge of Fh, shifting its IEP to more acidic values.

The negative surface charge of humic acid dramatically modifies the surface behavior of Fh (Fig. 2). In place of an IEP, the composite solid exhibits a high negative charge over the whole pH range. PO_4^{3-} increases negative surface charge relative to measurements recorded in NO_3^- media, showing even less dependence on pH. Particle size determination revealed that for Fh, HA-DIG and HA-DIG/Fh samples 81.3, 94.8 and 97.3 % of particles were larger than 20 μm, respectively.

3.2. Electrochemical studies

As previously reported by Antilen et al. (2016), CIPRO presents an irreversible oxidation process over glassy carbon electrodes if potential is fixed at around 1.0 V vs Ag|AgCl reference electrode by using CV at pH = 7.0 in PBS solution. This oxidation peak presents a current intensity that is directly proportional to CIPRO concentration in phosphate buffer solution (PBS). Accordingly, CIPRO concentration measurements obeyed a linear trend with current, following the equation

$$y = 0.0462[CIPRO] + 2.746" \ (R^2 = 0.999)$$

where CIPRO concentration is given in μmol L^{-1} and y corresponds to current (μA) in a cyclic voltammetry experiment at pH 7.0 (Antilen et al., 2016). Oxidation of CIPRO on the electrode surface is negligible compared to the concentration change during adsorption. Cyclic voltammograms at different concentrations of CIPRO and the corresponding calibration curve are presented in Supplementary Information (Figs. S1 and S2, respectively). Linearity is maintained for the range 30–300 μmol L^{-1} of CIPRO. For the square wave voltammetry technique, the current measurements were also proportional to the CIPRO concentration at pH = 7.0 in KNO_3 solution, with excellent linearity results for the range 30–300 μmol L^{-1} of CIPRO. The use of different electrochemical techniques in the analytical determination of CIPRO was a consequence of loss of sensitivity observed in the measurements with KNO_3 as the electrolyte anion. The loss of sensitivity can be explained by the dependence on the electrolyte used, which may affect the diffusion process of the analyte towards the working electrode surface-seems to be as one important electrochemical kinetics component-, which in the case of PBS, would be more efficient than KNO_3 (Bard and Faulkner, 2001), obtaining higher current values at same CIPRO concentrations. In this sense, when CV was used to quantify the analyte in the presence of KNO_3, no faradaic processes were observed in comparison to when PBS was used as supporting electrolyte. With the aim of suppressing the double layer capacitance and consequently the capacitive current, SWV was the appropriate technique when the electrolyte was KNO_3. This permitted recognition of the current signals associated to the CIPRO electroactivity as a faradaic process. All results are presented in Supplementary Information (voltammograms at different concentration of CIPRO, Fig. S3; and calibration curve, Fig. S4).

For both electrochemical techniques, the calibration curves (PBS and KNO_3 solution) were used to convert electrochemical current outputs directly into CIPRO concentration values, without the requirement of a solid-solution physical separation.

The results of the kinetic adsorption experiments were used to calculate the amount of adsorbed antibiotic as a function of the time. Fig. 3 shows CIPRO adsorption kinetics results with respective kinetics models fitting in each case. Kinetics for CIPRO adsorption behave differently over each adsorbent, with equilibration time of 45, 60 and 120 min for CIPRO adsorption over Fh, HA-DIG and HA-DIG/Fh, respectively. The pH values were constant with a maximum average fluctuation of 0.72 and 0.54 units in KNO_3 and PBS, respectively. These results indicate that adsorption occurs faster on the humic acid or iron oxide along compared to their composites.

The three materials showed differences in maximum adsorption of the antibiotic, with Fh, HA-DIG, and HA-DIG/Fh measuring 50, 120 and 110 μmol g^{-1}, respectively. Humic acid demonstrated the highest adsorption capacity compared to to the other adsorbents. These preliminary observations were corroborated by kinetic model adjustment

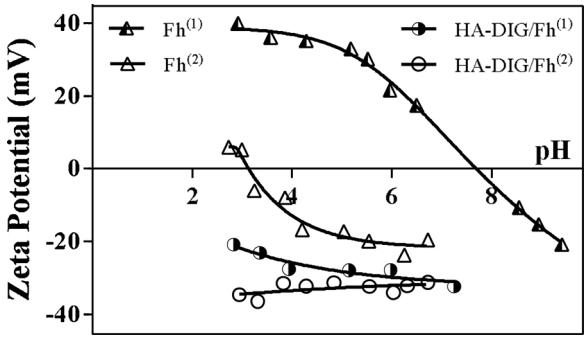

Fig. 2. Zeta potential vs pH curves for ferrihydrite (Fh) and composite HA-DIG/Fh, measured in (1) KNO_3 1.0 mM and in (2)KH_2PO_4.

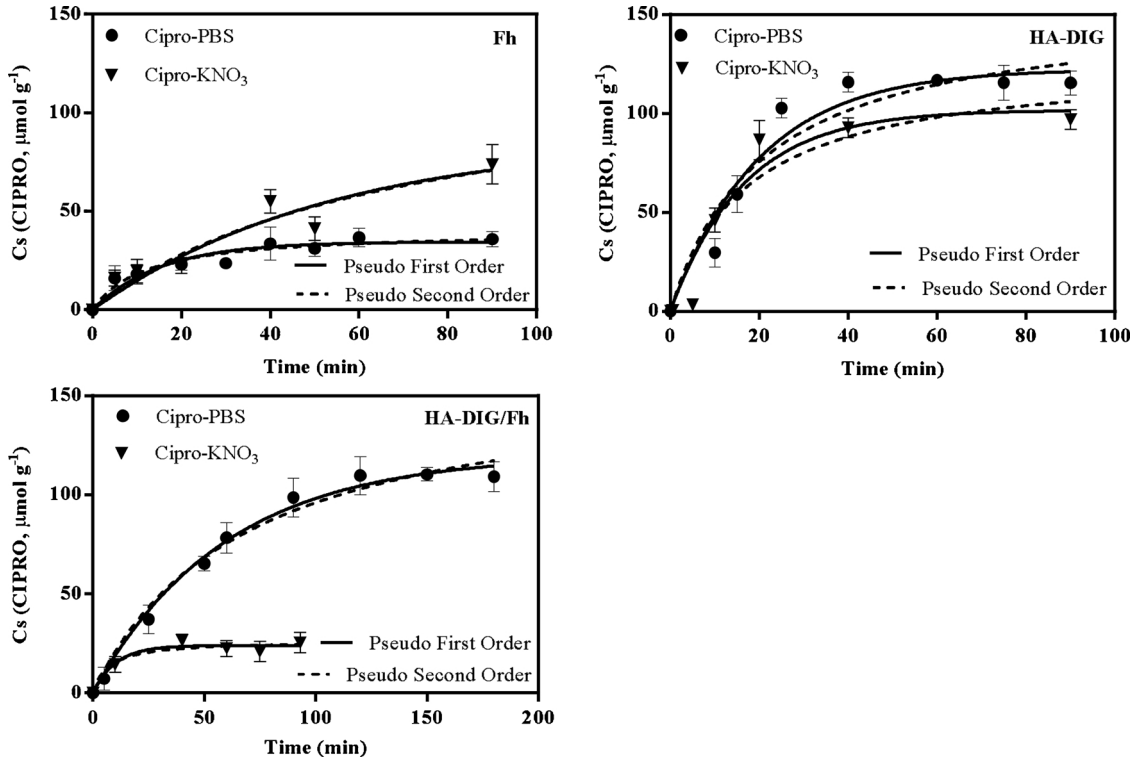

Fig. 3. Adsorption kinetics for CIPRO ($3{\cdot}10^{-4}$ mol L^{-1}) in KNO_3 and PBS on Fh, HA-DIG and HA-DIG/Fh with the respective kinetic model fitting.

Table 1
Kinetic models' parameters for adsorption of CIPRO in KNO_3 and PBS.

Pseudo 1st order model		Fh		HA-DIG		HA-DIG/Fh	
		PBS	KNO_3	PBS	KNO_3	PBS	KNO_3
C_m	µmol g^{-1}	34.5	87.3	122.4	101.8	120.2	23.9
k_1	min^{-1}	0.07	0.02	0.05	0.06	0.02	0.10
ε	%	0.05	0.25	0.13	1.12	0.08	0.08
R^2		0.911	0.912	0.950	0.936	0.993	0.955
		Pseudo 2nd order model					
C_m	µmol g^{-1}	40.4	125.1	154.2	126.5	161.7	26.4
k_2	g µmol^{-1} min^{-1}	12.1	68.5	20.8	17.4	68.4	7.1
ε	%	0.04	0.24	0.17	1.59	0.10	0.08
R^2		0.941	0.916	0.925	0.912	0.984	0.940

of experimental data. Table 1 shows the pseudo-first and pseudo-second order parameters and model fitting of kinetic adsorption data for both anions.

The determination coefficient (R^2) and standard error (ε) of fitting process were used as criteria to establish which model more accurately described the experimental data. In the case of adsorption on Fh, the pseudo-second order model better described the experimental data than pseudo-first order model (PBS), indicating that CIPRO adsorption occurs at two different sites of the iron oxide structure. On the other hand, adsorption on HA-DIG and HA-DIG/Fh was described more accurately by the pseudo-first order model. Therefore, adsorption process on single active sites of adsorbents seems more important.

Comparison of the reaction rate constants (k_1) for the adsorption of CIPRO (PBS) on HA-DIG and HA-DIG/Fh ($5.0{\cdot}10^{-2}$ and $1.7{\cdot}10^{-2}$ min^{-1} on HA-DIG and HA-DIG/Fh, respectively) revealed that the adsorption process occurred three times faster on humic acid compared to the composite. Comparing C_m values between adsorbent materials, HA-DIG and HA-DIG/Fh achieved the highest antibiotic adsorption per mass of adsorbent. While the composite materials reached equilibrium more slowly than humic acid, maximum adsorption of the antibiotic was comparable.

Next, adsorption isotherm experiments were carried out using NO_3^- and PO_4^{3-} as supporting electrolytes to compare their effect on adsorption. Fig. 4 presents the adsorption isotherms with different electrolyte backgrounds, PBSand KNO_3, and their fit using adsorption models. The pH values were constant with a maximum average fluctuation of 0.50 and 0.45 units for KNO_3 and PBS, respectively.

Classification of adsorption isotherm curves by their initial slope and shape (Giles and Smith, 1974) results in S-type curves for CIPRO adsorption on HA-DIG in both electrolytes and on HA-DIG/Fh in KH_2PO_4 as background electrolyte. This indicates a cooperative effect between solute molecules affecting the adsorption process on HA-DIG and HA-DIG/Fh. An L-type curve can be observed for HA-DIG/Fh in KNO_3, which results from the high affinity related to chemical sorption interaction.

In contrast to the composite materials, Fh displays an H-type isotherm for antibiotic adsorption in KNO_3. This observation indicates a high affinity between CIPRO molecules with active sites of ferrihydrite, which can be attributed to van der Waals forces acting during the adsorption process. However, the adsorption of CIPRO on Fh in KH_2PO_4 exhibits a C-type isotherm, corresponding to an initial slope with no adsorbate concentration dependence until the maximum adsorption has been reached, like as a partition coefficient (k_d) which is the ratio between the two phases of an adsorbate. This result can be explained by the two distinct adsorbent surface charges in the solution, which is corroborated by the different isoelectric point observed in results of zeta potential vs pH (Fig. 2). The zero point of charge is indicative of pH at which there is no net charge associated on the solid soil particles (Sposito, 1981). The distinct behavior of Fh variable surface charge active sites depending on the background electrolyte used indicates that in the case of PBS, Fh adsorbs chemical species ($H_2PO_4^-$ or HPO_4^{2-}, depending on the experimental pH), consequently modifying their surface and charge. In this way, the same adsorbent presents different surface charge at identical pH and ionic strength value, which would suggest that the electrostatic forces between CIPRO and the adsorbent are important in the adsorption process. Subsequently, the change in magnitude and even the sign of the surface charge (Fig. 2) modifies the

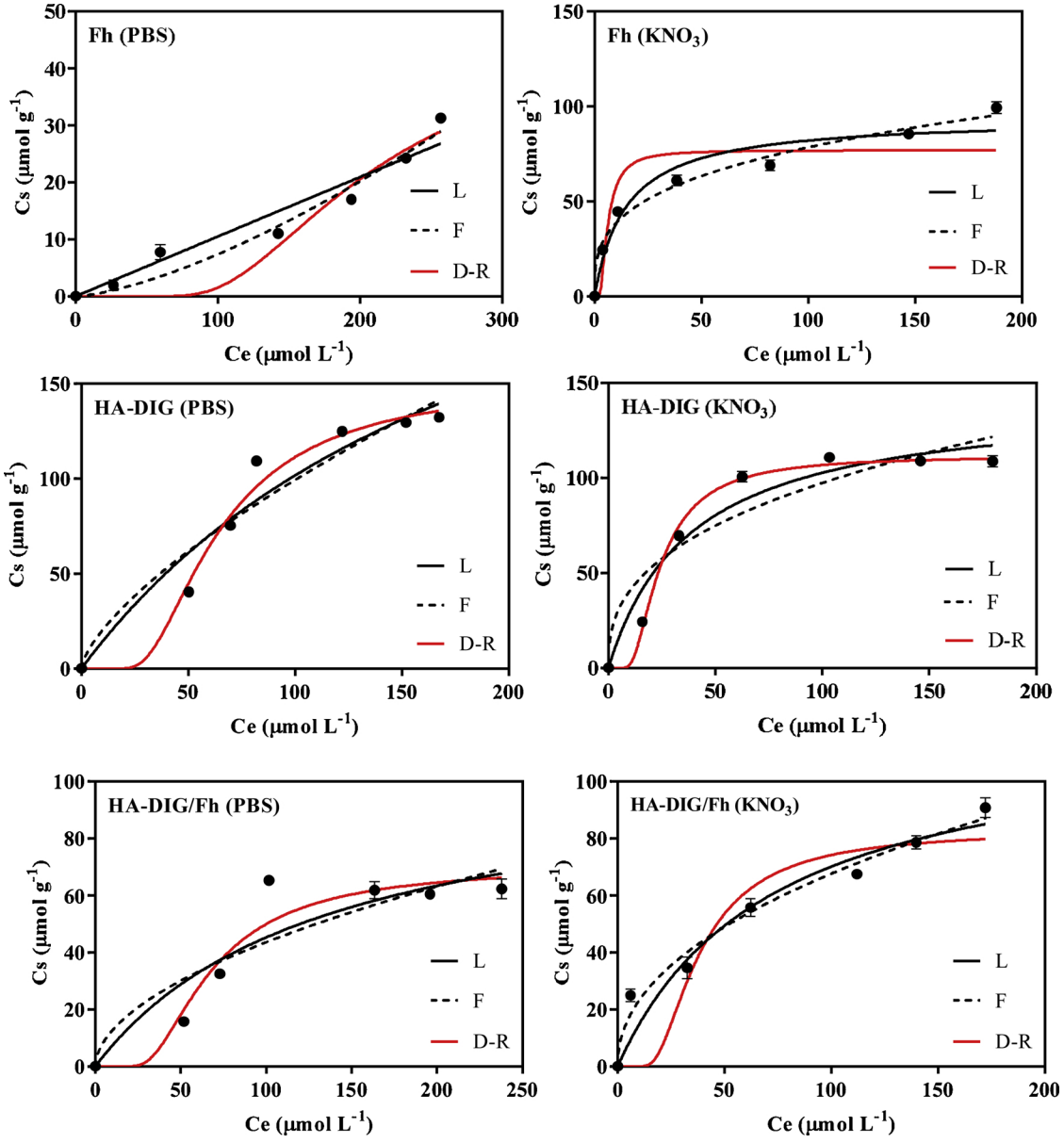

Fig. 4. Adsorption isotherms of CIPRO in PBS and KNO_3 (dots) and model fitting (lines).

Table 2
Models fitting parameters for CIPRO adsorption isotherms carried out in PBS.

Freundlich		Fh	HA-DIG	HA-DIG/Fh
K_F	µmol g^{-1}	0.009	4.190	3.692
n_{fads}		1.453	0.687	0.536
R^2		0.955	0.923	0.812
Langmuir				
$C_{m\text{-}cal}$	µmol g^{-1}	*ambiguous*	311	106
K_L	L µmol^{-1}	*ambiguous*	$4.86{\cdot}10^{-3}$	$7.47{\cdot}10^{-3}$
R^2		0.934	0.935	0.842
Dubinin-Radushkevich				
$C_{m\text{-}cal}$	µmol g^{-1}	49	152	70
K_{DR}	mol^2 J^{-2}	5716	508	563
E_{DR}	J mol^{-1}	9.4	31.4	29.8
R^2		0.897	0.984	0.932

K_{DR}: Dubinin-Radushkevich isotherm constant.
EDR: Free energy of adsorption.

Table 3
Models fitting parameters for CIPRO adsorption isotherms carried out in KNO_3.

Freundlich		Fh	HA-DIG	HA-DIG/Fh
K_F	µmol g^{-1}	18.9	16.9	7.6
n_{fads}		0.309	0.380	0.468
R^2		0.981	0.893	0.975
Langmuir				
$C_{m\text{-}cal}$	µmol g^{-1}	94	143	115
K_L	L µmol^{-1}	$6.77{\cdot}10^{-2}$	$2.59{\cdot}10^{-2}$	$1.46{\cdot}10^{-2}$
R^2		0.946	0.950	0.945
Dubinin-Radushkevich				
$C_{m\text{-}cal}$	µmol g^{-1}	77	112	83
K_{DR}	mol^2 J^{-2}	5.3	73.9	181.5
E_{DR}	J mol^{-1}	306.7	82.9	52.5
R^2		0.836	0.996	0.859

K_{DR}: Dubinin-Radushkevich isotherm constant.
EDR: Free energy of adsorption.

shape of the adsorption curve.

This change revealed that CIPRO will be adsorbed at pH 7.0 on Fh in KNO_3 solution with positive charge, while in contrast adsorption will occur on a negative surface charge in KH_2PO_4 media. When the negative surface charge of Fh increases the CIPRO adsorption could be increases too, even though the antibiotic is mainly found as zwitterion form at the pH studied. Collectively, these results demonstrate the effective of background electrolyte on adsorbent materials such as Fh. This effect is less pronounced in HA-DIG, where background electrolyte does not influence cooperative adsorption, but does increase the maximum adsorption of 100 μmol g^{-1} to 130 μmol g^{-1} for KH_2PO_4. Finally, in the case of the HA-DIG/Fh composite, the maximum adsorption in PBS is lower than that observed in the two other materials studied, representing the only case with lower adsorption in PBS than in KNO_3. This observation could result from lost adsorption sites in the synthesized material (Fh) into which these large biomacromolecules were incorporated (Wershaw, 1986). The SSA-BET area value obtained for the composite (2.41 ± 0.18 $m^2 g^{-1}$) with pore diameter of 13.7 nm and its evident decrease in comparison to the SSA-BET area of the Fh (81.88 ± 0.24 $m^2 g^{-1}$) with 4.4 nm supports this notion. In comparison, HA showed a very poor SSA-BET at 3.93 ± 0.26 $m^2 g^{-1}$.

The collective results from C_m values and adsorption curve shapes suggest that among the adsorbents studied, Fh exhibits the greatest potential for CIPRO remediation in aqueous media where $H_2PO_4^-$ or HPO_4^{2-} are present mainly. In addition to this qualitative analysis of the curves, Freundlich, Langmuir and Dubinin-Radushkevich models were applied to both describe the model and provide information about the adsorption mechanism involved. Models fitting parameters for CIPRO adsorption in PBS are presented on Table 2.

The determination coefficient (R^2) indicated that model fitting quality changed slightly depending on adsorbent, rendering the R^2 alone insufficient for model selection. Therefore, model selection was additionally based upon convergence of the calculations and agreement between calculated and experimental C_m. For instance, R^2 for CIPRO adsorption on Fh was similar when modelling with Freundlich (0.955) and Langmuir (0.934) while the Dubinin-Radushkevich adsorption model yielded a determination coefficient of 0.897. In this case, experimental values corresponded to the initial zone of adsorption, where the Freundlich model fits CIPRO adsorption data for Fh. On the other hand, CIPRO adsorption on HA-DIG and HA-DIG/Fh presents higher R^2 values when fitting the Dubinin-Radushkevich model with $C_{m\text{-}cal}$ values of 152 and 70 μmol g^{-1} which are close to the experimental data: 132 and 62 μmol g^{-1}, respectively. Hence, the Dubinin-Radushkevich model better fit the adsorption isotherms on HA-DIG and HA-DIG/Fh. The importance of the adjustment of the experimental data to the Dubinin-Raduskevich isotherm model is that this model performs the calculation of energy distribution on the surface of the adsorbent, allowing prediction of how CIPRO will interact with the different materials in our study. The calculation of the free energy of adsorption is described by the equation (Mutavdžić Pavlović et al., 2017):

$$E_{DR} = 1/ (2K_{DR})^{1/2}$$

This equation indicates that HA-DIG presents stronger adsorbate/adsorbent interactions according to maximum adsorption capacity ($C_{m\text{-}cal}$). As presented in Table 2, E_{DR} values for adsorption on Fh and HA-DIG/Fh are 9.4 and 29.8, respectively, signifying that the cooperativity adsorption process between CIPRO molecules is more important for HA-DIG/Fh.

Table 3 presents fitting parameters for isotherms in KNO_3. R^2 for CIPRO adsorption on Fh when modelling with Freundlich (0.981) was similar to the Langmuir adsorption model (0.946), while Dubinin-Radushkevich parameters were lower (0.836). Because of the L-type experimental isotherm observed, Langmuir model and parameters were considered. The $C_{m\text{-}cal}$ value of 94 μmol g^{-1} was close (5.3 %) to the experimental data (99.3 μmol g^{-1}). Additionally, CIPRO adsorption on Fh presented the largest K_L value (affinity constant) compared to the other two adsorbents.

In contrast, data adjustment for CIPRO adsorption on HA-DIG presented excellent R^2 values when fitting the Dubinin-Raduskevich model with $C_{m\text{-}cal}$ values of 112 μmol g^{-1} which were very close to the experimental data (109.3 μmol g^{-1}). Therefore, the Dubinin-Radushkevich model better fit the adsorption isotherms made on HA-DIG, while that the Fh shows the highest adsorption free energy (306.7 j mol^{-1}) followed by HA-DIG and HA-DIG/Fh.

4. Conclusions

Considering the physicochemical surface properties of each material, the impact on adsorption at different soil-solution conditions was established, to determine the best material as a potential adsorbent of Ciprofloxacin.

To this end, we first synthesized and characterized adsorbent materials by Mössbauer spectroscopy to confirm the presence of Fh, with isoelectric points indicating a high dependence on the sign and magnitude, especially for the synthetic iron oxide. Subsequently, we developed and implemented an analytical method for the determination of CIPRO in PBS and in KNO_3 using cyclic voltammetry and square wave voltammetry, respectively. Results indicating sensitivity based on electrolyte type informed the use of square wave voltammetry for the measurements of CIPRO in KNO_3.

Kinetic studies revealed different equilibrium times for the materials studied, electrolyte type bearing minimal effect on the HA-DIG composite, which registered the highest CIPRO adsorption. Adsorption studies established the differential effects of the KNO_3 and PBS electrolytes on the shape of the curve CIPRO adsorption, a finding attributable to the changes in magnitude of surface charge registered. Finally, this work highlights the need to consider the adjustment (determination coefficient), as well as the $C_{m\text{-}cal}$ when applying adsorption models in order to adequately compare adsorption constants obtained from the different materials. Collectively, these results point to HA-DIG as a potential adsorbent material in a medium soil solution with high phosphate ions content and in a medium mainly dominated by NO_3^-. However, considering the high affinity between HA-DIG and CIPRO, antibiotic transport could be possible if the compounds were adsorbed/complexed on the soluble organic matter present in the soil solution. The above increases the probability of dispersion of the pollutant in soil profile.

Declaration of Competing Interest

The authors declare that they have no known competing financial interests or personal relationships that could have appeared to influence the work reported in this paper.

Acknowledgements

Support from Fondecyt project 1130094, Puente 2018 (P1811), Dicyt–USACH 021742PA, Proyecto Fondo Fortalecimiento USA1799, Basal Funding for Scientific and Technological Centers of Excellence FB0807 CEDENNA and CONICYT PIA/ANILLO ACM 170002 are kindly acknowledged. We thank Alyssa Gurbe for support in language assistance.

Appendix A. Supplementary data

Supplementary material related to this article can be found, in the online version, at doi:https://doi.org/10.1016/j.jhazmat.2019.121520.

References

Ahmed, M.J., 2017. Adsorption of non-steroidal anti-inflammatory drugs from aqueous solution using activated carbons: review. J. Environ. Manage. https://doi.org/10.

1016/j.jenvman.2016.12.073.
Albero, B., Tadeo, J.L., Escario, M., Miguel, E., Pérez, R.A., 2018. Persistence and availability of veterinary antibiotics in soil and soil-manure systems. Sci. Total Environ. 643, 1562–1570. https://doi.org/10.1016/j.scitotenv.2018.06.314.
Anderson, G., Williams, E.G., Moir, J.O., 1974. A comparison of the sorption of inorganic orthophosphate and inositol hexaphosphate by six acid soils. J. Soil Sci. https://doi.org/10.1111/j.1365-2389.1974.tb01102.x.
Antilen, M., Bustos, O., Ramirez, G., Canales, C., Faundez, M., Escudey, M., Pizarro, C., 2016. Electrochemical evaluation of ciprofloxacin adsorption on soil organic matter. New J. Chem. 40. https://doi.org/10.1039/c6nj00207b.
Bard, A.J., Faulkner, L.R., 2001. Electrochemical Methods: Fundamentals and Applications. Wiley.
Bayrakci, M., Gezici, O., Bas, S.Z., Ozmen, M., Maltas, E., 2014. Novel humic acid-bonded magnetite nanoparticles for protein immobilization. Mater. Sci. Eng. C 42, 546–552. https://doi.org/10.1016/j.msec.2014.05.066.
Bouyoucos, G.J., 1934. A method for determining the degree of decomposition that unknown decayed vegetable organic materials have already undergone in nature. Soil Sci. 38, 477–482.
Boxall, A.B.A., Kolpin, D.W., Halling-Sørensen, B., Tolls, J., 2003. Peer Reviewed: Are Veterinary Medicines Causing Environmental Risks?.
Charuaud, L., Jarde, E., Jaffrezic, A., Thomas, M.F., Le Bot, B., 2019. Veterinary pharmaceutical residues from natural water to tap water: sales, occurrence and fate. J. Hazard. Mater. 361. https://doi.org/10.1016/j.jhazmat.2018.08.075.
Escudey, M., Galindo, G., Förster, J.E., Briceño, M., Diaz, P., Chang, A., 2001. Chemical forms of phosphorus of volcanic ash-derived soils in Chile. Commun. Soil Sci. Plant Anal. 32, 601–616. https://doi.org/10.1081/CSS-100103895.
Essington, M.E., 2004. Soil and Water Chemistry: an Integrative Approach. CRC Press, pp. 311–398. https://doi.org/10.1017/CBO9781107415324.004.
Evangelou, V.P., 1998. Environmental Soil and Water Chemistry: Principles and Applications.
Fao, N.J., Food, W.H.O., Programme, S., Alimentarius, C., Thirty, C., Rome, S., Of, R., Thirty, T.H.E., Session, F., The, O.F., Committee, C., Nutritionfoods, O.N., Special, F.O.R., Uses, D., Soden, B., 2013. Cl 2012/42-nfsdu. pp. 1–5.
Figueroa, R.A., Leonard, A., Mackay, A.A., 2004. Modeling tetracycline antibiotic sorption to clays. Environ. Sci. Technol. https://doi.org/10.1021/es0342087.
Freundlich, H.M., 1906. Uber die Adsorption in Losungen. Zeitschrift Für Phys. Chemie. 57, 385–470.
Fu, H., Li, X., Wang, J., Lin, P., Chen, C., Zhang, X., (Mel) Suffet, I.H., 2017. Activated carbon adsorption of quinolone antibiotics in water: performance, mechanism, and modeling. J. Environ. Sci. (China) 56, 145–152. https://doi.org/10.1016/j.jes.2016.09.010.
Giles, C.H., Smith, D., 1974. A general treatment and classification of the solute adsorption isotherm part I. Theoretical. J. Colloid Interface Sci. 47.
Gu, C., Karthikeyan, K.G., 2005a. Interaction of tetracycline with aluminum and iron hydrous oxides. Environ. Sci. Technol. 39, 2660–2667. https://doi.org/10.1021/es048603o.
Gu, C., Karthikeyan, K.G., 2005b. Sorption of the antimicrobial ciprofloxacin to aluminum and iron hydrous oxides. Environ. Sci. Technol. 39, 9166–9173. https://doi.org/10.1021/es051109f.
Ho, Y.S., McKay, G., 1999. Pseudo-second order model for sorption processes. Process Biochem. 34, 451–465. https://doi.org/10.1016/S0032-9592(98)00112-5.
Jacobsen, A.M., Halling-Sørensen, B., Ingerslev, F., Hansen, S.H., 2004. Simultaneous extraction of tetracycline, macrolide and sulfonamide antibiotics from agricultural soils using pressurised liquid extraction, followed by solid-phase extraction and liquid chromatography-tandem mass spectrometry. J. Chromatogr. A. https://doi.org/10.1016/j.chroma.2004.03.034.
Jiang, C., Zhang, X., Xu, X., Wang, L., 2016. Magnetic mesoporous carbon material with strong ciprofloxacin adsorption removal property fabricated through the calcination of mixed valence Fe based metal-organic framework. J. Porous Mater. 23, 1297–1304. https://doi.org/10.1007/s10934-016-0188-x.
John, J., McCarthy, M., Zachara, J.M., 1989. Subsurface transport of contaminants. Environ. Sci. Technol. 23, 752. https://doi.org/10.1021/es00065a001.
Kolpin, D.W., Furlong, E.T., Meyer, M.T., Thurman, E.M., Zaugg, S.D., Barber, L.B., Buxton, H.T., 2002. Pharmaceuticals, hormones, and other organic wastewater contaminants in U.S. streams, 1999-2000: a national reconnaissance. Environ. Sci. Technol. https://doi.org/10.1021/es011055j.
Lagergren, S., 1898. About the theory of so-called adsorption of soluble substances. K. Sven. Vetensk. Handl. 24 (4), 1e39.
Langmuir, I., 1918. The adsorption of gases on plane surfaces of glass, mica and platinum. J. Am. Chem. Soc. 410, 1361–1404.
Liang, Z., Zhaob, Z., Sun, T., Shi, W., Cui, F., 2016. Adsorption of quinolone antibiotics in spherical mesoporous silica: effects of the retained template and its alkyl chain length. J. Hazard. Mater. 305, 8–14. https://doi.org/10.1016/j.jhazmat.2015.11.033.
Lindsey, M.E., Meyer, M., Thurman, E.M., 2001. Analysis of trace levels of sulfonamide and tetracycline antimicrobials in groundwater and surface water using solid-phase extraction and liquid chromatography/mass spectrometry. Anal. Chem. https://doi.org/10.1021/ac010514w.
Liu, Z., Sun, P., Pavlostathis, S.G., Zhou, X., Zhang, Y., 2013. Adsorption, inhibition, and biotransformation of ciprofloxacin under aerobic conditions. Bioresour. Technol. 144, 644–651. https://doi.org/10.1016/j.biortech.2013.07.031.
Magistad, O.C., Reitemeier, R.F., 1943. Soil solution concentrations at the wilting point and their correlation with plant growth. Soil Sci. 55, 351–360. https://doi.org/10.1097/00010694-194305000-00002.
Marsac, R., Martin, S., Boily, J.F., Hanna, K., 2016. Oxolinic acid binding at Goethite and akaganéite surfaces: experimental study and modeling. Environ. Sci. Technol. 50, 660–668. https://doi.org/10.1021/acs.est.5b04940.
Misra, D.N., 1969. Adsorption on heterogeneous surfaces: a dubinin-radushkevich equation. Surf. Sci. 18, 367–372. https://doi.org/10.1016/0039-6028(69)90179-4.
Mutavdžić Pavlović, D., Ćurković, L., Grčić, I., Šimić, I., Župan, J., 2017. Isotherm, kinetic, and thermodynamic study of ciprofloxacin sorption on sediments. Environ. Sci. Pollut. Res. 24, 10091–10106. https://doi.org/10.1007/s11356-017-8461-3.
Schwertmann, R.M., Cornell, U., 2000. Iron Oxides in the Laboratory: Preparation and Characterization, Second edi. Wiley-VCH, Weinheim.
Sposito, G., 1981. The operational definition of the zero point of charge in soils 1. Soil Sci. Soc. Am. J. 45, 292–297.
Thiele-Bruhn, S., Beck, I.-C., 2005. Effects of sulfonamide and tetracycline antibiotics on soil microbial activity and microbial biomass. Chemosphere 59, 457–465. https://doi.org/10.1016/J.CHEMOSPHERE.2005.01.023.
Urdiales, C., Sandoval, M.P., Escudey, M., Pizarro, C., Knicker, H., Reyes-Bozo, L., Antilén, M., 2018. Surfactant properties of humic acids extracted from volcanic soils and their applicability in mineral flotation processes. J. Environ. Manage. 227, 117–123. https://doi.org/10.1016/j.jenvman.2018.08.072.
Vandenberghe, B.L., De Grave, R.E., Landuydt, C., 1990. Some aspects concerning the characterization of iron oxides and hydroxides in soils and clays. Hyperfine Interact. 53, 175.
Watanabe, A., Kuwatsuka, S., 1991. Fractionation of soil fulvic acids using polyvinyl -pyrrolidone and their lonization difference spectra. Soil Sci. Plant Nutr. 37, 611–617. https://doi.org/10.1080/00380768.1991.10416929.
Wershaw, R.L., 1986. A new model for humic materials and their interactions with hydrophobic organic chemicals in soil-water or sediment-water systems. J. Contam. Hydrol. 1, 29–45. https://doi.org/10.1016/0169-7722(86)90005-7.
Wershaw, S.E., Pinckney, R.L., Booker, D.J., 1977. Chemical structure of humic acids- 1. A generalized structural model. J. Res. U. S. Geol. Surv. 5, 565–569. (Accessed June 22, 2018). https://www-scopus-com.ezproxy.puc.cl/record/display.uri?eid=2-s2.0-0017530606&origin=resultslist&sort=plf-f&src=s&st1=Wershaw+R.L.&nlo=&nlr=&nls=&sid=adb66165eb0e5d1a94e0ab533644ee59&sot=b&sdt=cl&cluster=scopubyr%2C%221977%22%2Ct&sl=25&s=AUTHOR-NAME%28We.
Wu, Q.J., Zhou, Y.M., Wu, Y.N., Zhang, L.L., Wang, T., 2013. The effects of natural and modified clinoptilolite on intestinal barrier function and immune response to LPS in broiler chickens. Vet. Immunol. Immunopathol. https://doi.org/10.1016/j.vetimm.2013.02.006.